Journal of Chromatography A, 1217 (2010) 256–263

Contents lists available at ScienceDirect

Journal of Chromatography A

journal homepage: www.elsevier.com/locate/chroma

# Prediction of gas collection efficiency and particle collection artifact for atmospheric semivolatile organic compounds in multicapillary denuders

Mark D. Rowe, Judith A. Perlinger*

*Department of Civil and Environmental Engineering, Michigan Technological University, 1400 Townsend Dr., Houghton, MI 49931, USA*

ARTICLE INFO

*Article history:*
Received 2 October 2009
Received in revised form
12 November 2009
Accepted 16 November 2009
Available online 1 December 2009

*Keywords:*
Breakthrough
Collection efficiency
PCB
PBDE
Polydimethylsiloxane
Thermal desorption

ABSTRACT

A modeling approach is presented to predict the sorptive sampling collection efficiency of gaseous semivolatile organic compounds (SOCs) and the artifact caused by collection of particle-associated SOCs in multicapillary diffusion denuders containing polydimethylsiloxane (PDMS) stationary phase. Approaches are presented to estimate the equilibrium PDMS–gas partition coefficient ($K_{pdms}$) from a solvation parameter model for any compound, and, for nonpolar compounds, from the octanol–air partition coefficient ($K_{oa}$) if measured $K_{pdms}$ values are not available. These estimated $K_{pdms}$ values are compared with $K_{pdms}$ measured by gas chromatography. Breakthrough fraction was measured for SOCs collected from ambient air using high-flow (300 L min$^{-1}$) and low-flow (13 L min$^{-1}$) denuders under a range of sampling conditions (−10 to 25 °C; 11–100% relative humidity). Measured breakthrough fraction agreed with predictions based on frontal chromatography theory using $K_{pdms}$ and equations of Golay, Lövkvist and Jönsson within measurement precision. Analytes included hexachlorobenzene, 144 polychlorinated biphenyl congeners, and polybrominated diphenyl ethers 47 and 99. Atmospheric particle transmission efficiency was measured for the high-flow denuder (0.037–6.3 μm diameter), and low-flow denuder (0.015–3.1 μm diameter). Particle transmission predicted using equations of Gormley and Kennedy, Pich, and a modified filter model, agreed within measurement precision (high-flow denuder) or were slightly greater than (low-flow denuder) measured particle transmission. As an example application of the model, breakthrough volume and particle collection artifact for the two denuder designs were predicted as a function of $K_{oa}$ for nonpolar SOCs. The modeling approach is a necessary tool for the design and use of denuders for sorptive sampling with PDMS stationary phase.



## 1. Introduction

Semivolatile organic compounds (SOCs) partition between a gaseous fraction and a particle-associated fraction in the atmosphere. The SOCs include chemicals from a wide range of classes that originate from natural and anthropogenic sources, or are produced in the atmosphere as a result of oxidation processes, for example alkanes, alkenes, aromatic hydrocarbons, carbonyls, carboxylic acids, and organic nitrates [1,2]. These compounds are of current scientific interest for their participation in photochemical reactions that lead to formation of ozone and fine particulate matter [3]. SOCs have been implicated as a significant source of secondary organic aerosol particles that is not accounted for in current models [4]. Fine aerosol particles affect human health directly [5], and account for the greatest single contribution, among physical processes, to uncertainty in climate change predictions ([6], Fig. 2.20). The SOCs also include chemicals that are persistent, bioaccumulative, and toxic (PBT), such as polycyclic aromatic hydrocarbons (PAHs), polybrominated diphenyl ethers (PBDEs), organochlorine pesticides (OCPs), and polychlorinated biphenyls (PCBs). Gas-particle partitioning behavior plays an important role in prediction of fate and transport of SOCs in indoor [7] and outdoor [1] environments; deposition rates tend to be greater for the particle-associated fraction, while chemical transformation rates tend to be greater for the gaseous fraction. Sample collection techniques that can accurately separate gaseous from particle-associated SOCs are needed to monitor concentrations and predict behavior of SOCs in outdoor and indoor environments.

Conventional sampling techniques for SOCs, including the widely used high-volume sampler [8], involve collection of the particle-associated fraction on a filter located upstream of a sorbent bed that collects the gaseous fraction. This approach suffers from both positive and negative artifacts caused by volatilization of SOCs from particles on the filter, adsorption of gaseous SOCs onto the filter, or reaction of collected SOCs with atmospheric oxidizing species [9–11]. Diffusion denuders followed by filters in the sampling path have been developed as an alternative to avoid artifacts produced by the conventional filter-sorbent bed sampler

* Corresponding author. Tel.: +1 906 487 3641; fax: +1 906 487 2943.
*E-mail address:* jperl@mtu.edu (J.A. Perlinger).

0021-9673/$ – see front matter © 2009 Elsevier B.V. All rights reserved.
doi:10.1016/j.chroma.2009.11.049

[11–15]. Separation of gaseous and particulate analytes in a diffusion denuder is based on the greater diffusivity of gases compared to particles.

The two most common artifacts associated with denuder samplers are breakthrough of gaseous analytes from the denuder and particle collection within the denuder [16]. In fact, a small amount of breakthrough from the denuder can significantly bias a particulate-fraction measurement for SOCs that are lightly retained in the denuder and partition weakly to particles [17]. Similarly, collection of a small fraction of particles within the denuder can significantly bias the gaseous fraction for predominantly particle-associated analytes. Breakthrough artifacts can be avoided by selecting a sample volume that is less than the temperature- and analyte-specific breakthrough volume. The artifact due to particle collection within the denuder is a function of denuder design, analyte volatility, and ambient particle size distribution. It is necessary to predict the occurrence of these artifacts as a function of denuder design and sampling variables to minimize their impacts on data quality.

In this paper we present a practical approach to predict gaseous collection efficiency and particle collection artifact in multicapillary diffusion denuders that contain polydimethylsiloxane (PDMS) as sorbent. PDMS offers several advantages for sorptive sampling: (1) PDMS is a re-usable coating that is durable in both thermal desorption and solvent extraction methods, (2) PDMS collects analytes by non-selective absorption resulting in low risk of irreversible adsorption and catalytic surface reaction, (3) PDMS retains little water in sampling of humid air [18], thus minimizing difficulties caused by water in sample processing and analysis, (4) diffusivity in PDMS is high compared to other sorptive sampling polymers [19], leading to rapid uptake kinetics, and (5) PDMS coating has a smooth surface, compared to particulate coatings such as XAD, which may lower its potential to trap particles. In prior literature, measured gas collection efficiency has been reported under specific conditions [11,20], but an approach to predict collection efficiency in the denuder as a function of analyte properties, design, and sampling variables was not developed. Volckens and Leith [16] considered the effects of assumed gas and particle collection artifacts on measured gas-particle partition coefficients, but did not attempt to predict the magnitude of collection efficiency artifacts in the denuder. Baltussen et al. [21] described the application of chromatographic theory to predict gaseous collection efficiency in sorptive samplers, but use of this method is limited in practice because values of the temperature-dependent equilibrium stationary phase-gas partition coefficient are generally not available. We present two methods to estimate the PDMS–gas partition coefficient ($K_{pdms}$) and compare estimated to measured $K_{pdms}$ values for several SOCs. Additionally, an approach to predict gaseous SOC and particle collection efficiency is described, and predictions are compared to measured collection efficiencies for two denuder designs. Finally, an application of the model is presented in which the range of volatility over which sampling is predicted to be artifact-free is compared for the two denuder designs.

## 2. Theory

### 2.1. Prediction of gaseous collection efficiency

To predict gaseous collection efficiency using chromatographic theory, it is necessary to know the temperature-dependent $K_{pdms}$ for each analyte of interest. It is desirable to estimate this parameter to avoid the need to measure $K_{pdms}$ for each analyte. Using the solvation parameter model of Abraham et al. [22], an equilibrium liquid–gas partition coefficient is obtained by adding the contributions of the various molecular interactions:

$$\log(K) = c + eE + sS + aA + bB + lL \quad (1)$$

where $K$ is the liquid–gas partition coefficient, $c$ is the intercept, $e, E$ are the solvent, solute $n$- and $pi$–electron pair interaction descriptor, $s, S$ are the solvent, solute dipole/polarizability interaction descriptor, $a, A$ are the solvent hydrogen bond base, solute hydrogen bond acid interaction descriptor, $b, B$ are the solvent hydrogen bond acid, solute hydrogen bond base interaction descriptor, and $l, L$ are the solvent, solute cavity formation/dispersive interaction descriptor. In this model, the temperature dependence of $K$ is addressed through the use of temperature-dependent solvent descriptors, while solute descriptors are not varied with temperature. Measured solute descriptors are available for many compounds of interest (for example [22,23]), and a group contribution method can be used to estimate solute descriptors for any compound (Platts et al. [24] as implemented in [25]) if measured values are not available. We obtained temperature-dependent solvent descriptors for PDMS by linear regression of solvent parameters determined by Li et al. at five temperatures. Regression parameters and statistics are reported in Table 1, and details of the calculations are given in Supplemental Information. $K_{pdms}$ estimated using the parameters in Table 1 is compared to other estimates of $K_{pdms}$ in Section 4.1.

A brief description of the approach to predict gaseous collection efficiency is provided here with a detailed description and equations provided in Supplemental Information. Sorptive sampling of gases into a liquid phase in open tubular samplers can be described using chromatographic theory (for example [21]). Thermodynamic equilibrium between the two phases is described using the liquid–gas partition coefficient. PDMS may be treated as a liquid here, even though it is a cross-linked polymer, because chromatographic retention in PDMS is dominated by dissolution of analytes into the bulk phase rather than by interfacial adsorption. Interfacial adsorption can contribute significantly to retention at low temperatures and for analytes that differ significantly in polarity from the stationary phase [26]. For nonpolar stationary phases such as PDMS, adsorption at the substrate dominates over adsorption at the air–PDMS surface, and is greater if the substrate is not well deactivated. Therefore, interfacial adsorption may contribute to retention in sorptive samplers at ambient temperature. However, retention by adsorption is additive to retention by dissolution ([26], Eq. (9)); thus prediction of retention by partitioning into the bulk phase alone may be considered a lower bound to predicted retention. The lower limit of expected retention is of interest for the purpose of predicting collection efficiency.

The extent to which the collection efficiency is limited by longitudinal diffusion in the gas and the rate of mass transfer in gas and liquid is taken into account through the theoretical plate height, $H$, a length scale that is used to estimate the length of sampler over which equilibrium between the two phases is reached. $H$ is given as a function of flow velocity, diffusivity in the two phases, capillary diameter, and film thickness in the Golay equation [as in [27], p. 34].

**Table 1**
Linear regression parameters (slope and intercept) used to estimate temperature-dependent solvent descriptors for polydimethylsiloxane stationary phase for estimation of the liquid–gas partition coefficient by the solvation parameter model (Eq. (1)).

| | Slope[a] | Std. error | Intercept[a] | Std. error | $R^2$ |
|---|---|---|---|---|---|
| $c$ | 121.9 | 8.6 | −0.445 | 0.023 | 0.9854 |
| $s$ | – | – | 0.209 | 0.001 | – |
| $a$ | 273.5 | 15.8 | −0.509 | 0.043 | 0.9901 |
| $l$ | 439.1 | 0.6 | −0.613 | 0.002 | 1.0000 |

[a] $c, a, l$ = slope/$T$ + intercept, derived from the data of Li et al. [36], $n$ = 5, temperature range 60–140 °C. Descriptors $e$ and $b$ were equal to zero.

Diffusivity in PDMS was estimated using the empirical correlation of Malcolm et al. [28]. As the sampler reaches equilibrium with the incoming concentration, the analyte will eventually begin to break through. The integral breakthrough fraction, *bt*, is defined as the ratio of analyte mass that passed through the denuder to analyte mass that entered the denuder over the sampling period. To predict *bt* as a function of sample volume, *H*, and sampler length, we used the expression of Lövkvist and Jönsson ([29], Eq. (8)), which was derived for conditions of constant inlet concentration and samplers with small numbers of theoretical plates (<100).

### 2.2. Prediction of particle transmission efficiency

Unintentional particle collection within the multicapillary denuder by diffusion and gravitational sedimentation along the length of the capillaries was modeled after Gormley and Kennedy [30], and Pich [31], respectively. Flow was assumed to be laminar within the denuder. Reynolds numbers were 46 and 119 for the high-flow and low-flow denuders, respectively, compared to a minimum value of approximately 2300 for turbulent flow in a tube ([32], p. 330). Particle collection can occur at the entrance of the denuder where flow is split by the capillary walls through impaction, interception, and diffusion. Particle collection on the ends of the capillary tubes was estimated by modification of the single-fiber filter collection efficiency model described by Hinds ([33], p. 190). An equivalent fiber diameter was defined as the ratio of solid area of the denuder cross-section to the summed length of capillary walls. The expression for overall collection efficiency was modified to represent collection on a two-dimensional surface (the capillary ends). Details are provided in Supplemental Information. Particle collection by electrophoresis and thermophoresis was neglected.

## 3. Experimental methods

### 3.1. Low-flow and high-flow multicapillary diffusion denuders

Low-flow (13 L min$^{-1}$) denuders consisted of 289 sections of capillary GC columns (ZB-1, 0.530-mm inside dia., 100% PDMS, 5-μm film, Phenomenex) packed into a deactivated stainless steel tube (250-mm long, 13-mm inside dia.). Details of design, construction, and application of the low-flow denuders are given elsewhere [12,18]. A high-flow denuder was designed using the modeling approach described here with the goal of achieving 2–3-h breakthrough-limited sampling times at 300 L min$^{-1}$ for relatively low-$K_{pdms}$ PBTs such as α-HCH and HCB. Details of fabrication of the high-flow denuder and associated equipment are presented elsewhere [34]. Briefly, the high-flow denuders were constructed of welded stainless steel honeycombs (102-mm outside dia., 1.04-mm cell dia., 51-mm depth, Quality Honeycomb, Arlington, TX). The honeycombs were deactivated using the Sulfinert process (Restek, Bellefonte, PA), then coated in our lab with a 5-μm film of cross-linked and bonded PDMS stationary phase (Rtx-1, Restek). Two honeycomb disks were stacked in stainless steel sleeves to make an overall denuder length of 102 mm. One denuder was fabricated using a cordierite ceramic honeycomb (1.3 mm square cell, 76-mm deep, Applied Ceramics, Doraville, GA), which was also Sulfinert deactivated and coated with PDMS. Anodized aluminum sampler housings held the denuders and filter holder in place and sealed the flow path with PTFE and Viton gaskets. A mass-flow controlled vacuum motor (Tisch Environmental, Cleves, OH) provided flow. Inlets were designed after those of Liu and Pui [35] to protect the samplers from rain during sampling as well as to maximize coarse particle transmission.

### 3.2. Measurement of PDMS–gas partition coefficients by gas chromatography

$K_{pdms}$ values were determined by a series of GC retention time measurements collected at a minimum of four temperatures for relatively low-$K_{pdms}$ PCBs, OCPs, and PBDEs. In practice, the sample volume that can be collected without breakthrough is limited by the lowest $K_{pdms}$ analyte of interest. The retention factor, *k*, can be determined from retention time measurements as $k = (t_r - t_m)/t_m$, where $t_r$ is the retention time, $t_m$ is the column holdup time, and $K_{pdms} = k\beta$. Column holdup time was determined using detector response from the trace quantity of air that is introduced with a blank injection. In practice, retention times are converted to volumes using flow rate measured at the column outlet, corrected for pressure drop over the column and evaporation of water in the soap film flow meter. We followed the correction procedure of Poole ([27], p. 10). $\beta$ was calculated from capillary column dimensions and film thickness provided by the manufacturer. Measurements were conducted at a column flow velocity equal to the denuder sampling flow velocity, and also at one-half and one-tenth of the sampling flow velocity to confirm that measured $K_{pdms}$ was not affected by limited mass transport. The GC was an HP 5890 Plus with an electron capture detector ($H_2$ carrier gas, 300 °C inlet, 5 m column). The column was the same as that used to construct the low-flow denuders. The oven temperature was held constant during the GC run, and confirmed with an independent thermocouple.

### 3.3. Measurement of breakthrough fraction for gaseous analytes

Sample collection conditions spanned the range of anticipated sampling conditions (from −10 to 25 °C, from 11% to 100% relative humidity, from 2.7 to 111.6 m$^3$ sample volume; Table S3). Outdoor air samples were collected at two locations: at the Integrated Atmospheric Deposition Network (IADN) monitoring site at Eagle Harbor, MI and on the roof of the Dow Environmental Sciences and Engineering Building (DESEB), Michigan Technological University, Houghton, MI. Indoor air samples were collected in the DESEB and adjacent Dillman Hall.

Breakthrough samples were collected in duplicate (co-located samplers), and two field blanks were included with each experiment. Field blanks were subjected to identical processing steps as samples, including assembly and disassembly at the sample collection site, with the exception that air was not drawn through field blank denuders. Each breakthrough sample consisted of two denuders connected in series, with the backup denuder intended to capture breakthrough of ambient SOCs from the front denuder. The experimental breakthrough fraction, *bt*, was calculated as

$$bt = \frac{M_b}{M_f + M_b} \quad (2)$$

where $M_f$ and $M_b$ are the mass of analyte on the front and back denuders, respectively. Temperature and relative humidity were measured using a model HMP45C sensor (Vaisala). Flow rate, temperature, and relative humidity were recorded at 1-min intervals. Sample volume was calculated from the flow rate record and reported at standard conditions of 25 °C, 1 atm. Sample extraction, cleanup, GC analysis, and quality assurance procedures are described in detail elsewhere [18,34]. A gas-phase cleanup method [18] was used to remove the polar background matrix of oxidized organic compounds in air prior to analysis in order to improve signal-to-noise ratio and selectivity in analysis by electron capture detection. Polar organochlorine compounds, including HCH isomers, were removed by the cleanup method; therefore, breakthrough fraction measurements are not presented for these compounds. Analytes included hexachlorobenzene, 144 PCB congeners, and PBDEs 47 and 99. The following quality criteria were

applied in breakthrough fraction measurements: (1) $M_f$ greater than nine times method detection limit, (2) $M_f$ greater than five times the field blank concentration. The first criterion ensures that a non-detect in the backup denuder indicates a breakthrough fraction less than 0.1. Analyte masses were blank subtracted.

### 3.4. Measurement of particle transmission efficiency

A scanning mobility particle sizer (SMPS) optical particle counting instrument (Model 3071A-3025A, TSI) was used to measure fine particle size distributions (from 0.01 to 0.5 μm) downstream of the low-flow and high-flow denuders during sampling of ambient atmospheric aerosol on the DESEB roof. Coarse particle size distributions (from 0.5 to 20 μm) were measured using an aerodynamic particle sizer (APS; Model 3320, TSI). The aerosol sample flow of 1 and 5 L min$^{-1}$ for the SMPS and APS, respectively, was drawn just downstream of the high-flow and low-flow denuders using isokinetic inlets in order to avoid artifacts associated with flow distortion at the aerosol sample inlet.

To measure particle transmission, ambient aerosol particle size distributions were collected alternately with the denuder and with a blank denuder in the sampling train without changing the inlet geometry (3-min samples, SMPS; 5-min samples, APS). The blank denuder consisted of the outer stainless steel tube of a denuder not containing any capillaries. The fractional particle transmission through the denuder, $f_t$, was measured as

$$f_t = \frac{N_d}{N_b} \quad (3)$$

where $N_d$ is the particle count recorded during a sample with the denuder in place, and $N_b$ is the particle count recorded during a subsequent sample with the blank denuder in place. Samples with fewer than 25 counts were discarded to ensure that the Poisson error of the particle count was less than 20%. A series of 24 $f_t$ measurements was conducted to obtain a mean and 95% confidence interval for comparison with the predicted $f_t$.

## 4. Results and discussion

### 4.1. Measured and estimated PDMS–gas partition coefficients

$K_{pdms}$ at 25 °C estimated from GC measurements and from solvent descriptors from several sources were compared to determine whether consistent estimates were obtained. Solvent descriptors for PDMS were available from four investigations, each relying on a distinctly different experimental method: (1) Li et al. [36] measured $K_{pdms}$ for a diverse set of 41–63 compounds at 60, 80, 100, 120, and 140 °C by open tubular column GC; (2) Poole and Poole [37] measured $K_{pdms}$ at 121.4 °C by packed column GC at several levels of stationary phase loading to correct for effects of interfacial adsorption. Phase ratio was measured by exhaustive Soxhlet extraction; (3) Sprunger et al. [38] compiled literature values of $K_{pdms-gas}$ and $K_{pdms-water}$ from static equilibrium experiments using PDMS-coated solid phase microextraction (SPME) fibers near 25 °C. Solvent descriptors were reported for the "dry" data set ($K_{pdms-gas}$, 64 compounds) and the "wet" data set (78 compounds), in which $K_{pdms}$ was calculated from $\log(K_{pdms-gas}) = \log(K_{pdms-water}) - \log(K_{air-water})$; (4) Hierlemann et al. [39] measured $K_{pdms}$ for 33 compounds at 25 °C using polymer coated acoustic wave vapor sensors.

Interfacial adsorption is expected to be more significant for polar compounds in PDMS and at low temperatures [26]; thus, dipole/polarizability and hydrogen bonding descriptors (*s*, *a*, and *b*) may be expected to have higher values in experiments that were affected by interfacial adsorption. Solvent descriptors from the above four investigations are presented in Table S2 along with 25 °C descriptors estimated from the data of Li et al. using the regression of Table 1, and for dry octanol. The descriptors of Li et al. at 120 °C are in close agreement with those of Poole and Poole, which were corrected for effects of interfacial adsorption, thus it is likely that the descriptors of Li et al. were minimally affected by interfacial adsorption. The *e*, *s*, *b*, and *l* descriptors of Hierlemann et al. are in close agreement with the 25 °C descriptors derived from Li et al., while Hierlemann et al. reported a higher *a* descriptor. Hierlemann et al. suspected substrate effects as the cause of their high *a* descriptor.

Sprunger et al. found higher values of polar descriptors for PDMS than prior investigations. The difference between the dry and wet descriptors of Sprunger et al. is greater than the reported uncertainties for all descriptors except *c*, suggesting that the solvation characteristics of PDMS are affected by water or that error was introduced through estimation of $K_{pdms-gas}$ from $K_{pdms-water}$. The descriptors of Sprunger et al. indicate stronger dipole/polarizability (*s*) and hydrogen bonding (*a*, *b*) interactions than Li et al. and Hierlemann, in fact the wet hydrogen bond acid (*b*) descriptor of Sprunger et al. (0.650) is comparable to that of octanol (0.702) within the stated uncertainty. PDMS contains no acidic hydrogens, unless silanol groups are present, and several investigators have found $b = 0$ for PDMS and similar polysiloxane stationary phases [36,37,39,40].

Polysiloxane-coated GC columns have been shown to become more polar through use. Li and Poole [40] determined solvent descriptors for a performance-degraded PDMS-5% diphenylsiloxane column and found increased *s*, *a*, and decreased *l* relative to a new column of the same type ($b = 0$ for both), which they attributed to greater analyte–substrate interaction in the degraded column.

Comparison of PDMS solvent descriptors determined by various methods leads us to interpret the descriptors of Li et al. as being representative of dissolution into pure PDMS, while those of Sprunger et al. may be more representative of PDMS in the presence of moisture, silanol, or other polar contaminants. The latter conditions may occur in a denuder during sampling or after a denuder has experienced several thermal desorption cycles, which may cause greater retention for polar compounds than predicted by the descriptors of Li et al. However, we cannot test this hypothesis here because we have not measured breakthrough for polar compounds in denuders. The descriptors of Li et al. likely represent a lower limit for retention of polar compounds in these denuders.

Regression parameters to calculate $K_{pdms}$ values as a function of temperature, derived from GC measurements, are presented in Table 2. $\log(K_{pdms})$ values at 25 °C estimated from GC measurements (using Table 2) and the solvent descriptors of Li et al. (using Table 1) are compared to $\log(K_{pdms})$ estimated using the solvent descriptors of Sprunger et al. in Table 3. The octanol–air partition coefficient, $\log(K_{oa})$, is presented for comparison [41–43]. $K_{pdms}$

**Table 2**
Regression parameters (slope and intercept) used to calculate temperature-dependent liquid–gas partition coefficients for polydimethylsiloxane stationary phase derived from GC retention time measurements. Standard errors of estimation of the slope and intercept by regression are given along with the coefficient of determination ($R^2$), number of observations ($n$), and the temperature range of the measurements.

| | Slope[a] | Std. error | Intercept[a] | Std. error | $R^2$ | $n$ | Temp. range (°C) |
|---|---|---|---|---|---|---|---|
| HCB | 3131 | 11 | −4.08 | 0.030 | 0.9998 | 21 | 60–140 |
| α-HCH | 3132 | 13 | −4.15 | 0.034 | 0.9997 | 21 | 60–140 |
| γ-HCH | 3220 | 13 | −4.25 | 0.034 | 0.9997 | 21 | 60–140 |
| PCB 18 | 3270 | 15 | −4.26 | 0.038 | 0.9995 | 26 | 80–180 |
| PCB 44 | 3580 | 18 | −4.64 | 0.045 | 0.9994 | 25 | 80–180 |
| PCB 65 | 3517 | 17 | −4.51 | 0.043 | 0.9994 | 25 | 80–180 |
| PBDE 28 | 3852 | 20 | −4.83 | 0.049 | 0.9995 | 20 | 100–180 |

[a] $\log(K_{pdms}) = \text{slope}/T + \text{intercept}$.

**Table 3**
Log($K_{pdms}$) at 25 °C estimated from GC measurements and from PDMS solvent descriptors from two sources. Percent difference is given between $K_{pdms}$ estimated from GC measurements and the various solvent descriptors. Log($K_{oa}$) at 25 °C is shown for comparison.

| Source | HCB | α-HCH | γ-HCH | PCB 18 | PCB 44 | PCB 65 | PBDE 28 |
|---|---|---|---|---|---|---|---|
| GC (Table 2)[a] | 6.42 | 6.35 | 6.55 | 6.70 | 7.37 | 7.28 | 8.09 |
| Li et al. (Table 1)[b] | 6.53 | 6.53 | 6.75 | 6.68 | 7.43 | 7.40 | 8.87 |
| Pct. diff. Li et al.—GC | 29 | 50 | 58 | −5 | 14 | 33 | 501 |
| Dry PDMS–gas [c] | 6.48 | 6.71 | 6.95 | 6.74 | 7.48 | 7.46 | 9.01 |
| Pct. diff. dry—GC | 14 | 126 | 154 | 8 | 28 | 50 | 730 |
| Wet PDMS-gas[c] | 6.31 | 6.70 | 6.95 | 6.73 | 7.44 | 7.42 | 8.98 |
| Pct. diff. wet—GC | −23 | 124 | 153 | 6 | 18 | 38 | 679 |
| Log($K_{oa}$) | 7.35 | 7.37 | 7.83 | 7.49 | 8.29 | 8.23 | 9.41 |

[a] Regression parameters derived from GC measurements of this work.
[b] Solvent descriptors derived from GC measurements of Li et al. [36].
[c] PDMS solvent descriptors reported by Sprunger et al. [38].

derived from Li et al. and from Sprunger et al. are equally comparable to $K_{pdms}$ derived from GC measurements for the relatively nonpolar HCB and PCBs. For the hydrogen bond basic HCHs, $K_{pdms}$ from Sprunger et al. is greater than both the $K_{pdms}$ derived from Li et al. and the GC measurements, which stems from the non-zero hydrogen bond acid descriptor of Sprunger et al. Neither source of solvent descriptors produced $K_{pdms}$ in good agreement with GC measurements for PBDE 28, although the value of Li et al. was closest, which may stem from the fact that solute descriptors for PBDE 28 were estimated from a group contribution method [25]. The root mean square (RMS) error between $K_{pdms}$ 25 °C derived from GC measurements and from Li et al. was 36% relative to the GC value and excluding PBDE 28, while $K_{pdms}$ varies over more than three orders of magnitude for the analytes included in Table 3 over typical sample collection temperatures (Table S3).

Log($K_{pdms}$) values derived from GC measurements were approximately one log unit less than log($K_{oa}$) at 25 °C (mean 1.03, std. error 0.07, $n = 7$) for the analytes tested, consistent with greater ease of cavity formation, *l*, dipole interactions, *s*, and hydrogen bond acid interactions, *b*, indicated by the solvent descriptors of octanol relative to those of PDMS (Table S2). Thus, an approximate value of $K_{pdms}$ at 25 °C for relatively nonpolar compounds similar to those listed in Table 3 may be obtained through the relationship $\log(K_{pdms}) \approx \log(K_{oa}) - 1$, which is plotted along with measured $K_{pdms}$ in Fig. S1. This relationship is not expected to hold for compounds more polar than those listed in Table 3; thus $K_{pdms}$ derived from measurements or estimated by the solvation parameter model should be used whenever possible.

### 4.2. Comparison of measured to predicted breakthrough fraction

The performance of the model for gaseous collection efficiency was evaluated by comparison of modeled to measured breakthrough fraction for low-flow and high-flow denuders under the experimental conditions listed in Table S3. Samples were collected in relatively pristine rural environments as well as in indoor environments having 10–100 times greater concentrations of SOCs [18]. Sample volumes were selected using the breakthrough model to give a value of *bt* in Eq. (2) of ~0.25 for HCB at the anticipated sample collection temperature; thus, breakthrough was expected only for analytes with relatively low-$K_{pdms}$. Valid measurements of *bt* values (non-zero breakthrough and meeting the quality criteria) were obtained for HCB and PCBs 6, 8, 17, and 18. Zero breakthrough fraction was predicted for compounds with greater $K_{pdms}$ than PCB 17 (log($K_{pdms}$) 25 °C = 6.71 using Table 1) under all conditions tested. For analytes with predicted $bt = 0$, measured $bt > 0.1$ was observed for only 11 of 243 and 12 of 58 measurements for low-flow and high-flow denuders, respectively.

Measured and predicted *bt* values are compared in Fig. 1. The solvation model was used to estimate $K_{pdms}$ values for PCBs 6, 8, and 17. In these experiments, the model was effectively used to select sample volumes that resulted in $bt < 0.4$ for HCB (Fig. 1) under all conditions. The RMS error between predicted and measured *bt* was 0.05 ($n = 28$) for the low-flow denuder, compared to a RMS difference of 0.05 ($n = 13$) between duplicate measurements, indicating that the model predicted breakthrough as well as can be evaluated given the precision of the measurements. The model predicted *bt* slightly less accurately for the high-flow denuder (RMS of 0.10, $n = 23$ vs. 0.05, $n = 7$ for duplicates). Several factors may have contributed, including less chromatographic efficiency of the high-flow denuders (6.5 theoretical plates vs. 12 for low-flow), band broadening caused by the gap between the two honeycombs that make up a metallic honeycomb high-flow denuder, non-uniform flow across the 102-mm dia. denuder, or non-uniform stationary phase coating. Breakthrough was predicted as well for the ceramic honeycomb (RMS 0.10, $n = 7$) as for the metallic honeycombs (RMS 0.10, $n = 16$), and for high humidity (RH > 70%) as for low humidity samples (Table S5).

### 4.3. Comparison of measured to predicted particle transmission

Predicted coarse particle transmission was much less for the low-flow than for the high-flow denuder (Fig. 2), primarily due to the gravitational sedimentation term. The low-flow denuder has previously been used for analytes that have a negligible particle-associated fraction, thus it was evaluated in a horizontally oriented aspirated sampler housing with an inlet that is designed to exclude coarse particles consisting of a 25-mm dia. pipe with a 90° bend [44]. Denuders should be oriented vertically for applications in which coarse particle transmission is of concern. Predicted impaction and interception losses on the capillary ends were enhanced in the low-flow denuder relative to the high-flow denuder due to higher face velocity (1.7 vs. 0.7 m $s^{-1}$) and greater capillary wall thickness (180 vs. 68 μm). The discontinuity in the modeled coarse particle transmission (visible in Fig. 2) occurs at the particle diameter for which the sum of interception and impaction collection efficiency reaches its theoretical maximum. In the low-flow denuder, measured particle transmission was slightly less than predicted for most size classes (Fig. 2), however mean particle transmission generally followed the decreasing trends in predicted transmission for fine particles (collection by diffusion) and coarse particles (sedimentation, impaction, and interception).

Measured particle transmission did not differ significantly from predicted particle transmission for nearly all size classes in the high-flow denuder (Fig. 2). High-flow fine particle transmission measurements were combined for the ceramic honeycomb and stainless steel honeycomb ($n = 24$ each); the two honeycomb support materials behaved similarly with respect to fine particle transmission.

The experimental method that we used to measure particle transmission allowed us to measure transmission of actual ambient aerosol particles under realistic sampling conditions over the

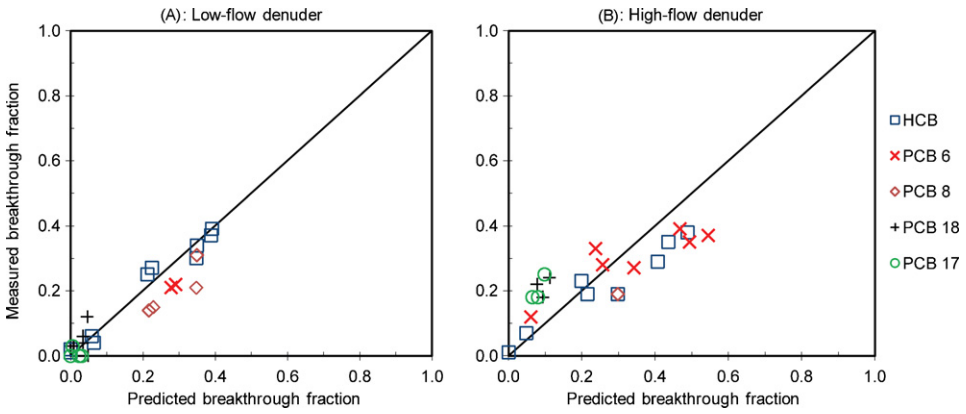


**Fig. 1.** Comparison of measured to predicted breakthrough fraction for low-flow (A) and high-flow denuders (B).

particle diameter range in which ambient aerosol particles are most numerous. However, the method had limited ability to verify model predictions for coarse particle transmission. Coarse particle number concentrations are relatively low, thus few of the samples had statistically significant numbers in size classes >∼2 μm. Coarse particles were detected in significant numbers up to 6.3 μm in the high-flow denuder vs. 3.1 μm in the low-flow denuder, reflecting the fact that the high-flow sampler inlet was designed to maximize coarse particle transmission while the low-flow inlet was designed to exclude coarse particles.

### 4.4. Application of the model to predict sampling artifacts

To estimate the magnitude of the artifact caused by unintentional particle collection in the denuder, model rural and urban log-normal aerosol particle size distributions were considered having properties given in Table S4 [45]. Predicted particle transmission efficiency through high-flow or low-flow denuders for each of the three aerosol modes (nucleation, accumulation, and coarse) was calculated

$$f_{tj} = \sum_{i=1}^{n} C_{pi} f_{ti} \tag{4}$$

where $f_{tj}$ is the mass fraction of particles transmitted through the denuder for a given aerosol mode $j$, $C_{pi}$ is the mass concentration of particles within a particle size class from the model distribution, and $f_{ti}$ is the fractional transmission for the size class from the model described above. The subscript $i$ indicates summation over particle diameter classes in an aerosol mode. The magnitude of the artifact caused by collection of particle-associated SOCs was then calculated

$$f_d = \frac{\sum_{j=1}^{3} K_{pj} C_{pj} (1 - f_{tj})}{\sum_{j=1}^{3} K_{pj} C_{pj} (1 - f_{tj}) + 1} \tag{5}$$

where $f_d$ is the mass fraction of SOC in the denuder sample associated with particles, $C_{pj}$ is the mass concentration of particles within aerosol mode $j$, and $f_{tj}$ is the fractional transmission for the aerosol mode (Eq. (4)). For the three aerosol modes, $f_{tj}$ was 0.93, 0.90 (nucleation), 0.98, 0.97, (accumulation), and 0.93, 0.40 (coarse) for high-flow and low-flow denuders, respectively, for the urban aerosol ($f_{tj}$ values were similar for rural aerosol, Table S4).

The particle-gas partition coefficient, $K_p$, was calculated after Harner and Shoeib [43], as a function of $K_{oa}$ and the fraction organic matter, $f_{om}$, of the aerosol particles. Arp et al. [46] calibrated a modified Abraham solvation parameter model to predict $K_p$, and found that under dry conditions for nonpolar and most polar compounds, sorption is dominated by absorption into a water-insoluble organic phase, while under moist conditions polar and ionized compounds can partition additionally into a mixed-aqueous phase. The model of Harner and Shoeib was selected because it is consistent with the mechanism identified by Arp et al. for nonpolar compounds, and facilitates the comparison of predicted performance for two denuder designs presented in Fig. 3 for the relatively nonpolar analytes considered here. The model of Arp et al. could be substituted for that of Harner and Shoeib in the approach presented here if a more mechanistically realistic prediction of particle collection artifact is desired for polar and ionized organic compounds under moist conditions.

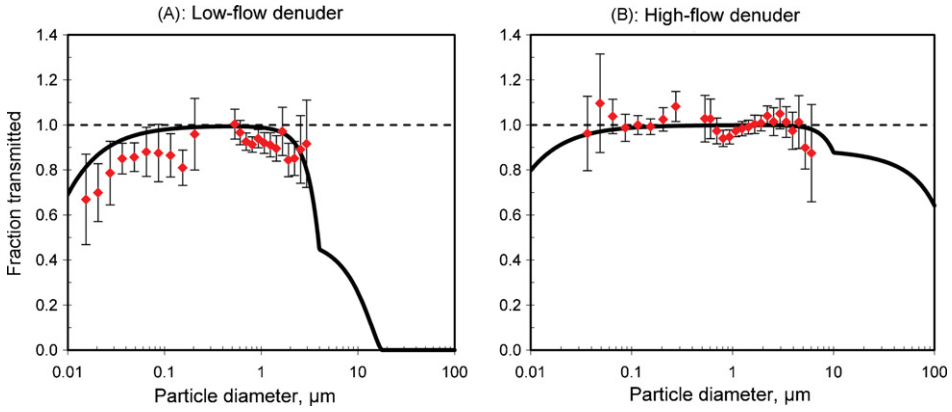


**Fig. 2.** Comparison of measured (symbols) to predicted (line) aerosol particle transmission through low-flow (A) and high-flow (B) denuders. Error bars represent the 95% confidence interval for the mean value, with $n = 24$ in most cases.

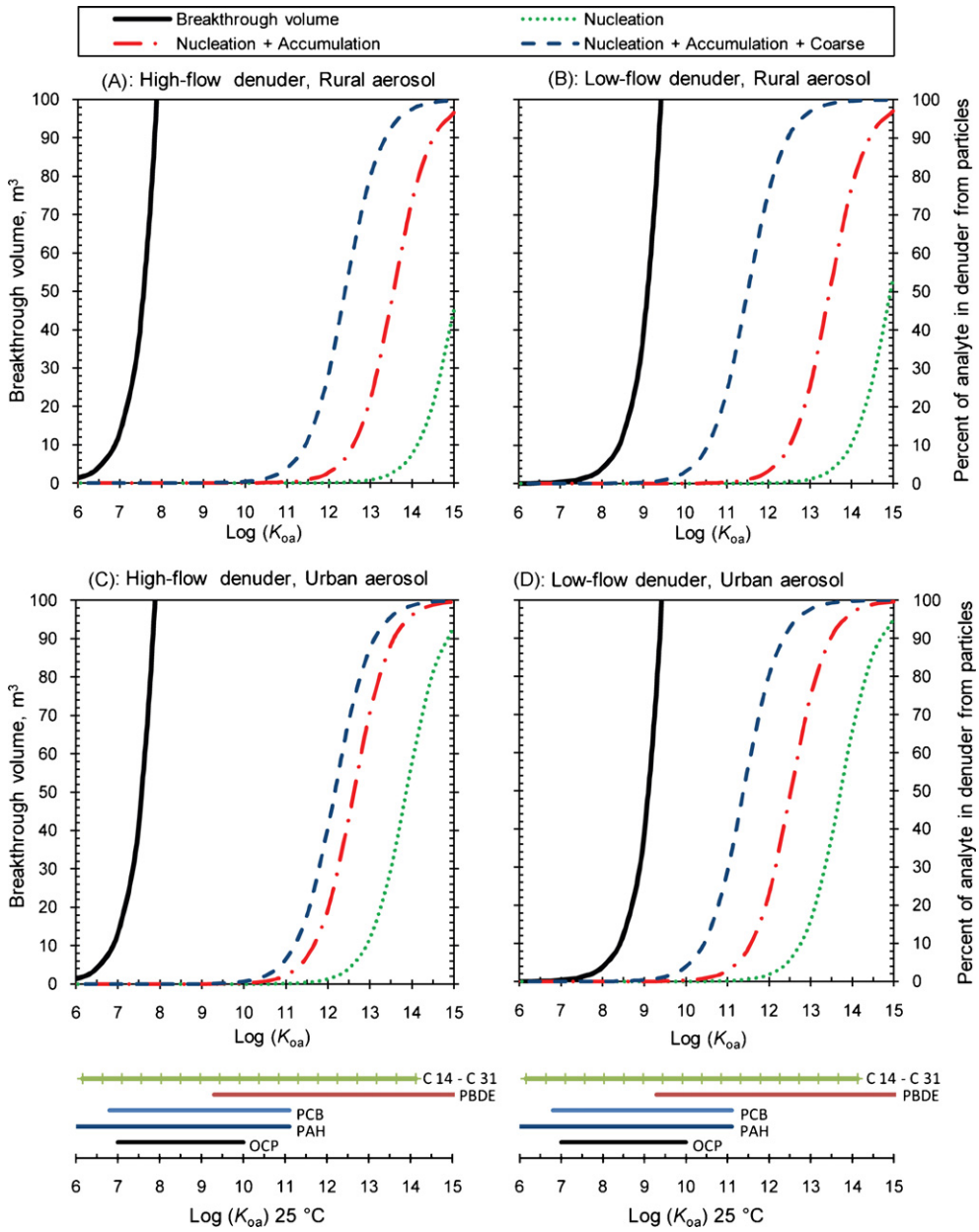


**Fig. 3.** Predicted breakthrough volume and particle collection artifact, $f_d$, for rural (A and B) and urban (C and D) aerosol particle size distributions in high-flow (A and C) and low-flow (B and D) denuders as a function of the octanol–air partition coefficient. Breakthrough volume is defined as the sample volume at which fractional breakthrough, $bt = 0.1$. The cumulative contribution of each aerosol mode to $f_d$ is plotted individually. The artifact-free operation range for the denuder is the region between the "Breakthrough volume" and "Nucleation + Accumulation + Coarse" lines in the figure. Ranges of $\log(K_{oa})$ for classes of SOCs are shown for reference (bottom).

In the Harner and Shoeib model, $f_{om}$ was assumed to be 0.23, 0.20, and 0.18 for the nucleation, accumulation, and coarse aerosol modes [47]. These values of $f_{om}$ result in a relatively uniform distribution of SOC mass fraction over fine and coarse particle modes, although $f_{om}$ could be manipulated in the model to estimate $f_d$ for SOCs that are not uniformly distributed among fine and coarse particles. The various classes of SOCs may favor either fine or coarse particles, depending on their source and $K_p$. SOCs that actively partition between the gas and particle fractions (low $K_p$) are likely to be found in both fine and coarse particle modes [48,49]. SOCs that are almost entirely particle-associated are likely to remain with their original source particles, for example association of PBDE 209 with coarse dust particles [50] and association of large molecular mass PAH and PCDD/F with fine combustion particles [48].

Breakthrough volume and $f_d$ values are a function of SOC $K_{pdms}$ and $K_p$, respectively, which are related to the common scale of $K_{oa}$ here (a relationship that is expected to hold for nonpolar SOCs only). The SOC volatility range over which a denuder can be used to separate gaseous and particle-associated SOCs and to collect gaseous SOCs is limited in the low-$K_{pdms}$ extreme by breakthrough volume and in the high-$K_p$ extreme by $f_d$. This relationship can be used to create a window of effective phase separation and gaseous SOC collection with a particular denuder, as illustrated in Fig. 3 for the high- and low-flow denuders. In Fig. 3, the relationship $\log(K_{pdms}) \approx \log(K_{oa}) - 1$ was assumed for breakthrough volume calculation. The breakthrough volume curve is shifted to the left for the high-flow denuder, relative to the low-flow denuder, while $f_d$ values are similar for the two, meaning that the high-flow denuder can sample over a wider range of SOC $K_{pdms}$ and $K_p$ values. Ranges of $K_{oa}$ values for classes of SOCs are shown in Fig. 3 for reference (C14–C31 *n*-alkanes [25], mono-octa CBs, OCPs, one to five ring PAHs [41], and tri-deca BDE [43,51 p. 30].

At 25 °C, the high-flow denuder can sample most PCBs, OCPs, PAHs, and lower-$K_p$ PBDEs at 20 $m^3$ breakthrough volume or higher and less than 10% $f_d$. The low-flow denuder is more limited in terms of breakthrough volume for lower-$K_{pdms}$ SOCs. The low-flow denuder is best applied when SOC mass is measurable in a sample of a few cubic meters, or when higher-$K_{pdms}$ SOCs are the target analytes and $f_d$ is not a concern. The cumulative contribution of each aerosol mode to $f_d$ is plotted separately in Fig. 3. It is apparent that the SOC volatility range over which artifact-free sampling can be conducted with the denuders can be expanded by excluding the coarse aerosol mode with an impactor or appropriate inlet design; however, a fraction of analyte in the sample may be lost unless the contents of the impactor are included in the analysis.

## Acknowledgements

Funding for this work was provided by the Great Lakes Commission. Fritz Burt and Juan Pablo Alvarez Rosario assisted with particle transmission measurements. Eric Bradfish, Shannon Flynn, and Kenny Papes assisted with flow rate calibration and field work. The comments of several anonymous reviewers improved the quality of this manuscript.

## Appendix A. Supplementary data

Supplementary data associated with this article can be found, in the online version, at doi:10.1016/j.chroma.2009.11.049.

## References

[1] E.L. Atlas, S.M. Li, L.J. Standley, R.A. Hites, in: C.N. Hewitt, W.T. Sturges (Eds.), Global Atmospheric Chemical Change, Elsevier Applied Science, New York, 1993, pp. 313–382.
[2] R. Fischer, R. Weller, H. Jacobi, K. Ballschmiter, Chemosphere 48 (2002) 981.
[3] S. Fuzzi, M.O. Andraea, B.J. Huebert, M. Kulmala, T.C. Bond, M. Boy, S.J. Doherty, A. Guenther, M. Kanakidou, K. Kawamura, V.M. Kerminen, U. Lohmann, L.M. Russell, U. Poschl, Atmos. Chem. Phys. 6 (2006) 2017.
[4] A.L. Robinson, N.M. Donahue, M.K. Shrivastava, E.A. Weitkamp, A.M. Sage, A.P. Grieshop, T.E. Lane, J.R. Pierce, S.N. Pandis, Science 315 (2007) 1259.
[5] C.A. Pope, D.W. Dockery, J. Air Waste Manage. 56 (2006) 709.
[6] IPCC, in: S. Solomon, D. Qin, M. Manning, Z. Chen, M. Marquis, K.B. Averyt, M. Tignor, H.L. Miller, (Eds.), Contribution of Working Group I to the Fourth Assessment Report of the Intergovernmental Panel on Climate Change, Cambridge, UK and New York, NY, USA, 2007, p. 996.
[7] C.J. Weschler, W.W. Nazaroff, Semivolatile organic compounds in indoor environments, Atmos. Environ. 42 (2008) 9018–9040.
[8] T.F. Bidleman, C.E. Olney, Environ. Contam. Toxicol. 11 (1974) 442.
[9] H.P.H. Arp, R.P. Schwarzenbach, K.U. Goss, Atmos. Environ. 41 (2007) 8241.
[10] M. Goriaux, B. Jourdain, B. Tmime, J.L. Besombes, N. Marchand, A. Albinet, E. Leoz-Garziandia, H. Wortham, Environ. Sci. Technol. 40 (2006) 6398.
[11] B.T. Mader, R.C. Flagan, J.H. Seinfeld, Environ. Sci. Technol. 35 (2001) 4857.
[12] D.E. Tobias, J.A. Perlinger, P.S. Morrow, P.V. Doskey, D.L. Perram, J. Chromatogr. A 1140 (2007) 1.
[13] L.A. Gundel, V.C. Lee, R.R. Kariyawasam, R.K. Stevens, J.M. Daisey, Atmos. Environ. 29 (1995) 1719.
[14] D.J. Eatough, in: D.A. Lane (Ed.), Gas and Particle Phase Measurements of Atmospheric Organic Compounds, Gordon and Breach Science Publishers, Amsterdam, The Netherlands, 1999, pp. 233–285.
[15] M.S. Krieger, R.A. Hites, Environ. Sci. Technol. 26 (1992) 1551.
[16] J. Volckens, D. Leith, Atmos. Environ. 37 (2003) 3385.
[17] T.F. Bidleman, R.L. Falconer, T. Harner, in: D.A. Lane (Ed.), Gas and Particle Phase Measurements of Atmospheric Organic Compounds, Gordon and Breach Science Publishers, Amsterdam, 1999, pp. 39–71.
[18] M.D. Rowe, J.A. Perlinger, J. Chromatogr. A 1216 (2009) 5940.
[19] T. Rusina, F. Smedes, J. Klanova, K. Booij, I. Holoubek, Chemosphere 68 (2007) 1344.
[20] M.S. Krieger, R.A. Hites, Environ. Sci. Technol. 28 (1994) 1129.
[21] E. Baltussen, C.A. Cramers, P.J.F. Sandra, Anal. Bioanal. Chem. 373 (2002) 3.
[22] M.H. Abraham, S.C. Harpreet, G.S. Whiting, R.C. Mitchell, J. Pharm. Sci. 83 (1994) 1085.
[23] M.H. Abraham, J.M. Al-Hussaini, J. Environ. Monit. 7 (2005) 295.
[24] J.A. Platts, M.H. Abraham, D. Butina, A. Hersey, J. Chem. Inf. Comp. Sci. 40 (2000) 71.
[25] Pharma Algorithms, ADME Boxes version 3.5; ABSOLV module, 2006.
[26] C. Poole, S. Poole, J. Chromatogr. A 1216 (2009) 1530.
[27] C.F. Poole, The Essence of Chromatography, Elsevier, Amsterdam, 2003.
[28] K. Malcolm, D. Woolfson, J. Russell, P. Tallon, L. McAuley, D. Craig, J. Control. Release 90 (2003) 217.
[29] P. Lövkvist, J.A. Jönsson, Anal. Chem. 59 (1987) 818.
[30] P.G. Gormley, M. Kennedy, P. Royal Irish Acad. 52A (1949) 163.
[31] J. Pich, J. Aerosol Sci. 3 (1972) 351.
[32] F.M. White, Fluid Mechanics, McGraw-Hill, New York, 1999.
[33] W.C. Hinds, Aerosol Technology, John Wiley & Sons, New York, 1999.
[34] M.D. Rowe, J.A. Perlinger, Environ. Sci. Technol., submitted for publication.
[35] B.Y.H. Liu, D.Y.H. Pui, Atmos. Environ. 15 (1981) 598.
[36] Q. Li, C.F. Poole, W. Kiridena, W.W. Koziol, Analyst 125 (2000) 2180.
[37] S.K. Poole, C.F. Poole, J. Chromatogr. A 697 (1995) 425.
[38] L. Sprunger, A. Proctor, W. Acree Jr., M. Abraham, J. Chromatogr. A 1175 (2007) 162.
[39] A. Hierlemann, E. Zellers, A. Ricco, Anal. Chem. 73 (2001) 3458.
[40] Q. Li, C. Poole, J. Sep. Sci. 24 (2001) 129.
[41] A. Beyer, F. Wania, T. Gouin, D. Mackay, M. Matthies, Environ. Toxicol. Chem. 21 (2002) 941.
[42] N. Li, F. Wania, Y.D. Lei, G.L. Daly, J. Phys. Chem. Ref. Data 32 (2003) 1545.
[43] T. Harner, M. Shoeib, J. Chem. Eng. Data 47 (2002) 228.
[44] J.A. Perlinger, D.E. Tobias, P.S. Morrow, P.V. Doskey, Environ. Sci. Technol. 39 (2005) 8411.
[45] K.J. Whitby, Atmos. Environ. 12 (1978) 135.
[46] H. Arp, R. Schwarzenbach, K. Goss, Environ. Sci. Technol. 42 (2008) 5541.
[47] J.H. Offenberg, J.E. Baker, Environ. Sci. Technol. 33 (1999) 3324.
[48] H. Kaupp, M.S. McLaughlan, Atmos. Environ. 34 (2000) 73.
[49] T.M. Holsen, K.E. Noll, S.P. Liu, W.J. Lee, Environ. Sci. Technol. 25 (1991) 1075.
[50] B.H. Wilford, G.O. Thomas, K.C. Jones, B. Davidson, D.K. Hurst, Environ. Int. 34 (2008) 412.
[51] M.D. Rowe, Modeling contaminant behavior in Lake Superior: a comparison of PCBs, PBDEs, and mercury, M.S. Thesis, Michigan Technological University, 2009, 61 pp, http://gradworks.umi.com/1464086.pdf.